

ARTICLE



# Cholesterylation of Smoothed is a calcium-accelerated autoreaction involving an intramolecular ester intermediate

Ao Hu<sup>1,5</sup>, Jing-Zan Zhang<sup>2,5</sup>, Jie Wang<sup>2</sup>, Chen-Chen Li<sup>2</sup>, Meng Yuan<sup>1</sup>, Gang Deng<sup>1</sup>, Zi-Cun Lin<sup>1</sup>, Zhi-Ping Qiu<sup>1</sup>, Hu-Yue Liu<sup>1</sup>, Xian-Wei Wang<sup>2,3</sup>, Peng-Cheng Wei<sup>1</sup>, Xiao He<sup>2,4</sup>, Xiaolu Zhao<sup>1</sup>, Wen-Wei Qiu<sup>2</sup> and Bao-Liang Song<sup>1</sup>

© CEMCS, CAS 2022

Hedgehog (Hh) is a morphogen that binds to its receptor Patched 1 and activates Smoothed (SMO), thereby governing embryonic development and postnatal tissue homeostasis. Cholesterol can bind and covalently conjugate to the luminal cysteine-rich domain (CRD) of human SMO at the D95 residue (D99 in mouse). The reaction mechanism and biological function of SMO cholesterylation have not been elucidated. Here, we show that the SMO-CRD undergoes auto-cholesterylation which is boosted by calcium and involves an intramolecular ester intermediate. In cells, Hh stimulation elevates local calcium concentration in the SMO-localized endosomes through store-operated calcium entry. In addition, we identify the signaling-incompetent SMO D95E mutation, and the D95E mutant SMO can bind cholesterol but cannot be modified or activated by cholesterol. The homozygous *Smo<sup>D99E/D99E</sup>* knockin mice are embryonic lethal with severe developmental delay, demonstrating that cholesterylation of CRD is required for full-length SMO activation. Our work reveals the unique autocatalytic mechanism of SMO cholesterylation and an unprecedented role of calcium in Hh signaling.

Cell Research (2022) 32:288–301; <https://doi.org/10.1038/s41422-022-00622-0>

## INTRODUCTION

The Hedgehog (Hh) signaling pathway is a tightly regulated intercellular communication system that governs the developmental events in most multicellular eukaryotic organisms. Hh pathway also modulates regeneration and homeostasis in adult tissues, whereas misactivated Hh signaling leads to certain cancers, including basal cell carcinoma and medulloblastoma.<sup>1–5</sup> Smoothed (SMO) is a G-protein coupled receptor (GPCR)-like signal transducer, which is indispensable for transducing the extracellular Hh ligand signal across the plasma membrane (PM). SMO is inhibited by Patched 1 (PTCH1) when Hh is absent. Hh binds to PTCH1 and relieves the suppression on SMO. The activated SMO translocates to the primary cilium, regulates post-translational processing of glioma-associated oncogene homolog (GLI) transcription factors, and ultimately upregulates the expression of downstream genes.<sup>4,6–8</sup>

Cholesterol, the most abundant sterol in mammalian cells, plays critical roles in Hh signaling. On one hand, the linkage of cholesterol to the carboxyl terminus of the mature Hh protein facilitates its secretion.<sup>9–11</sup> On the other hand, the Hh-receiving cells require cholesterol to activate SMO to transduce the signal.<sup>12–15</sup> Recent structural studies have revealed multiple sterol binding sites in the SMO protein.<sup>12,13,16,17</sup> We have found that cholesterol not only binds to the N-terminal cysteine-rich domain (CRD) of SMO, but also covalently conjugates to the 95<sup>th</sup> aspartic acid residue (Asp95 or D95),<sup>14,18</sup> which resides in the deep bottom

of the cholesterol-binding groove in CRD.<sup>14</sup> The knockin mice lacking the SMO cholesterylation site (*Smo<sup>D99N/D99N</sup>*) are embryonic lethal, fully resembling the phenotypes of *Smo*-null mice.<sup>14,19</sup> EBP, an enzyme in cholesterol biosynthesis, can bind to SMO and inhibit cholesterylation likely through blocking SMO budding from ER.<sup>20</sup> As the D95N mutation of human SMO abolishes both cholesterol binding and modification, it is unknown that whether SMO is activated by cholesterol binding or cholesterol conjugation. Another pivotal yet unresolved question is how SMO cholesterylation occurs.

## RESULTS

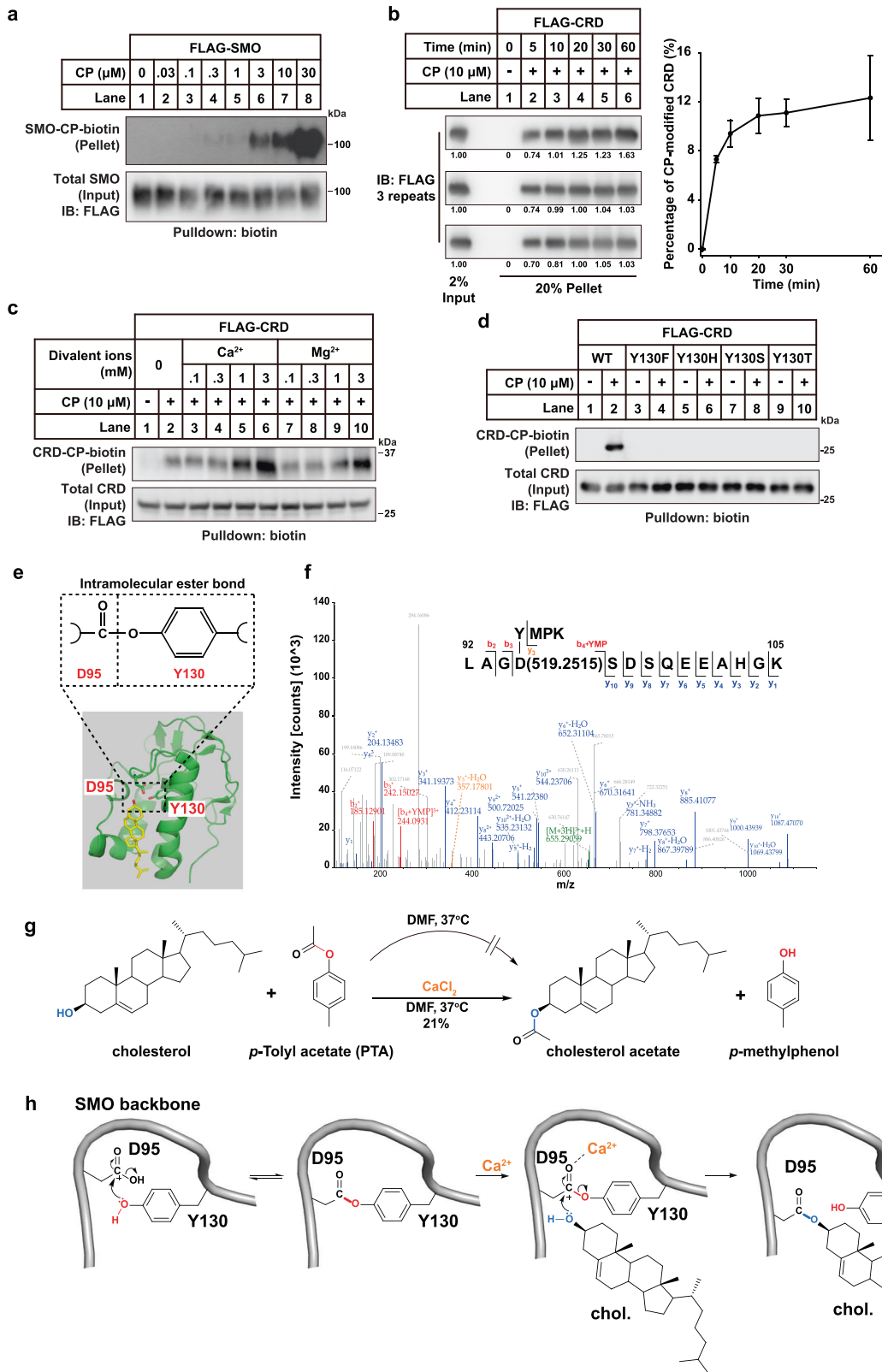
### Cholesterylation of SMO is an autoproducting event enhanced by Ca<sup>2+</sup>

In order to search for the factors required for SMO cholesterylation, we established an in vitro assay depicted in Supplementary information, Fig. S1a with the attempt to reconstitute SMO cholesterylation. The immunopurified FLAG-tagged SMO was incubated with the cholesterol-derived CP probe in the buffer containing 0.2% *n*-Dodecyl- $\beta$ -D-maltoside (DDM). Click chemistry was carried out subsequently to link biotin alkyne to allow enrichment by neutravidin beads. Figure 1a showed that CP modified SMO in a concentration-dependent manner. The SMO (D95N) mutant was not conjugated by CP (Supplementary information, Fig. S1b), suggesting that the in vitro modification

<sup>1</sup>The Institute for Advanced Studies, Hubei Key Laboratory of Cell Homeostasis, College of Life Sciences, TaiKang Center for Life and Medical Sciences, TaiKang Medical School, Wuhan University, Wuhan, Hubei, China. <sup>2</sup>Shanghai Engineering Research Center of Molecular Therapeutics and New Drug Development, School of Chemistry and Molecular Engineering, East China Normal University, Shanghai, China. <sup>3</sup>College of Science, Zhejiang University of Technology, Hangzhou, Zhejiang, China. <sup>4</sup>NYU-ECNU Center for Computational Chemistry at NYU Shanghai, Shanghai, China. <sup>5</sup>These authors contributed equally: Ao Hu, Jing-Zan Zhang. <sup>✉</sup>email: zhaoxiaolu@whu.edu.cn; wwqiu@chem.ecnu.edu.cn; blsong@whu.edu.cn

Received: 16 July 2021 Accepted: 10 January 2022

Published online: 4 February 2022



is specific on D95. Addition of cytosol, ATP or GTP had no obvious effect on the cholesterylation of SMO (Supplementary information, Fig. S1c, d), and the reaction tolerated a pH range from 5.0–8.5 (Supplementary information, Fig. S1e). These results indicate that neither cytosolic factor nor energy is required for SMO

cholesterylation. To further simplify the assay, we used the purified CRD of SMO (SMO-CRD) to replace full-length SMO and performed *in vitro* cholesterylation assay. Similarly, the SMO-CRD was modified by CP in a time-dependent fashion (Fig. 1b). The *in vitro* cholesterylation showed fast kinetics, which reached a

**Fig. 1 Cholesterylation of SMO is an autoprocessing event enhanced by  $\text{Ca}^{2+}$ .** **a** The purified FLAG-SMO was modified by the cholesterol-azide probe CP in a concentration-dependent manner. **b** Time course of in vitro cholesterylation of SMO-CRD. Quantification was performed based on the band intensities of three independent experiments. Mean values  $\pm$  SD were shown. **c** The effect of  $\text{Ca}^{2+}$  and  $\text{Mg}^{2+}$  ions on the cholesterylation of SMO-CRD in vitro. **d** Y130 mutants of SMO-CRD were not modified by CP in vitro. **e** Illustration of the structure of SMO-CRD with cholesterol based on PDB: 5L7D. The intramolecular ester bond formed between the side chains of D95 and Y130 is shown at the top. **f** Mass spectrum of the purified SMO-CRD protein digested by trypsin and elastase. An adduct of 519.2515 Da (the YMPK fragment) was detected on D95 indicating a D95–Y130 covalent linkage. The  $b_4 + \text{YMP}$  ion denoted the YMP fragment linked to  $b_4$  ion (LAGD), which was generated from breakages between both D95/S96 and P132/K133 in MS/MS. The  $y_3$  ion in orange denoted the fragment ion from peptide YMPK which was linked to D95. **g** Chemical simulation of D95–Y130 to D95–cholesterol ester exchange using PTA and cholesterol as substrates in the presence or the absence of  $\text{CaCl}_2$  as catalyst. **h** A proposed reaction mechanism of the intramolecular ester bond formed between D95 and Y130, and the ester exchange for cholesterol modification.

plateau at ~20 min and about 10% of total SMO-CRD was modified (Fig. 1b). In cultured cells, about 4.7% of SMO was modified by CP in steady state (based on the band intensities in Supplementary information, Fig. S1g,  $0.63/20\% \times 1.5\% = 4.7\%$ ). The molar ratio of endogenous cholesterol and exogenously added CP was 4.267:1 (Supplementary information, Fig. S1h). The SMO-CP conjugation was enhanced by cholesterol depletion and competed off by cholesterol (Supplementary information, Fig. S1i, j). Thus, it could be estimated that about 24.8% of SMO was covalently modified by cholesterol and CP when Hh is absent ( $4.7\% \times (4.267 + 1) = 24.8\%$ ), assuming cholesterol and CP behave similarly in cells.<sup>14</sup> However, this number is highly variable and dependent on cholesterol and Hh levels. We further tested different divalent ions in SMO cholesterylation assay. Strikingly, calcium dramatically boosted the cholesterylation whereas magnesium had modest effect (Fig. 1c; Supplementary information, Fig. S1f).  $\text{Ca}^{2+}$  was able to enhance SMO cholesterylation at a concentration of 1 mM, around the same magnitude of that in the endoplasmic reticulum (ER) lumen in cells.<sup>21</sup>

To our knowledge, the carboxyl group usually does not directly condense with the hydroxyl moiety of cholesterol in cells. Instead, an intermediate is required for esterification. For example, fatty acids need to be converted to acyl-CoA before they esterify with cholesterol to make cholesteryl esters.<sup>22,23</sup> Similarly, does a high-energy reaction intermediate exist in the cholesterylation of SMO? As Y130 was critical for in vitro modification (Fig. 1d) and spatially close to D95, we therefore hypothesized that the D95 and Y130 might form an intermediate joint by an ester bond (Fig. 1e). To test this hypothesis, we performed mass spectrometry (MS) analysis on the SMO-CRD protein, which can spontaneously undergo cholesterylation in vitro. The SMO-CRD protein was expressed in cells, immunopurified, digested by trypsin and elastase and subjected to LC-MS/MS. The backbone fragment (L92 to K105) was detected. Importantly, a smaller fragment (Y130 to K133) was found to be covalently linked to the D95 residue by an ester bond joining Asp and Tyr side chains (Fig. 1f). Similarly, we detected a linkage of the dipeptide (D95–S96) to the peptide backbone (V129 to R138), further validating the covalent linkage between D95 and Y130 (Supplementary information, Fig. S2a). The calculated ester bond energy between D95 and cholesterol after covalent linkage is  $-96.5$  kcal/mol, which is 4.3 kcal/mol lower than that of the intramolecular ester bond between D95 and Y130 ( $-92.2$  kcal/mol) (Supplementary information, Fig. S2b–d). So, the transesterification reaction to cholesterol from the D95–Y130 ester bond is energetically favorable, supporting the hypothesis that D95–Y130 ester bond serves as a high-energy intermediate. Mutations of Y130 to histidine, serine or threonine failed to restore the cholesterylation, highlighting the importance of phenolic hydroxyl (Fig. 1d).

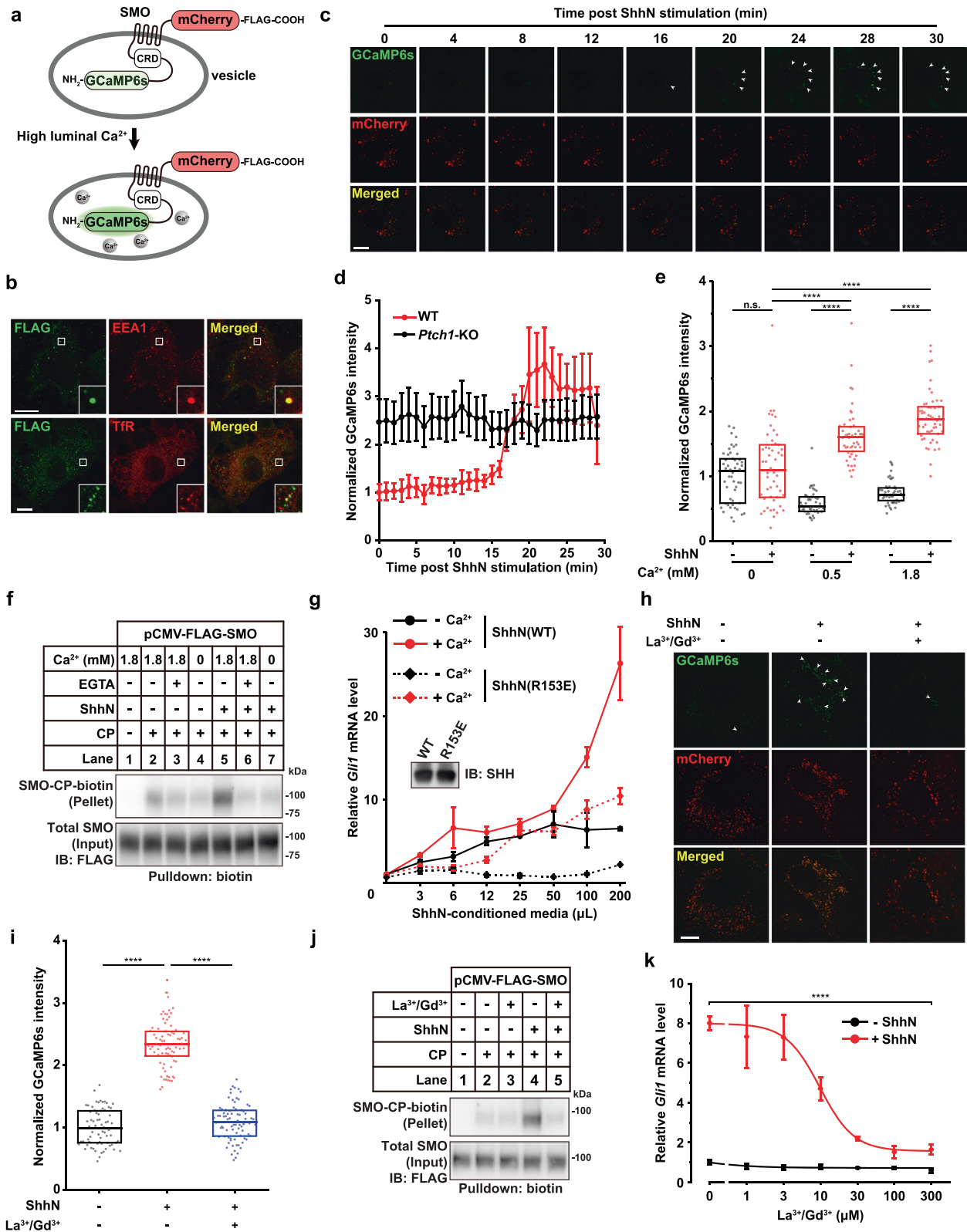
How can calcium ion accelerate SMO cholesterylation? It may do so by promoting the D95–Y130 ester formation, the transesterification from D95–Y130 to D95–cholesterol, or both. We used MS/MS to quantify the D95–Y130 ester bond and found that  $\text{Ca}^{2+}$  did not affect the percentage of D95–Y130 linkage (Supplementary information, Fig. S2e). As *p*-tolyl acetate (PTA) can

chemically simulate the ester bond between the side chains of D95 and Y130, we then incubated PTA with cholesterol at 37 °C to analyze the transesterification (Fig. 1g). There was no reaction at all when calcium was absent. Surprisingly, cholesterol acetate formed with 21% conversion rate when  $\text{CaCl}_2$  was present (Fig. 1g). Collectively, these results suggest that the D95–Y130 ester bond is an active intermediate for SMO cholesterylation, and the transesterification from D95–Y130 to D95–cholesterol is promoted by calcium (Fig. 1h).

### Hh stimulation increases $\text{Ca}^{2+}$ concentration ( $[\text{Ca}^{2+}]$ ) in SMO-localized endosomes

As Hh stimulates SMO cholesterylation,<sup>14</sup> we next asked whether  $\text{Ca}^{2+}$  fluctuation plays a role in SMO cholesterylation and activation under physiological conditions. We fused a genetically encoded calcium indicator, GCaMP6s, to the N-terminus of SMO to monitor the changes of CRD-local  $[\text{Ca}^{2+}]$  upon Hh treatment. Meanwhile, a mCherry fluorescent protein was attached to the C-terminus of SMO to generate a ratiometric calcium reporter (Fig. 2a). The GCaMP6s-SMO-mCherry reporter could translocate to primary cilia in response to 4-hour treatment of N-terminal domain of Sonic Hh (ShhN), SAG and cyclopamine (Supplementary information, Fig. S3a), resembling wild-type (WT) SMO. The fluorescent proteins did not alter the cholesterylation of SMO either (Supplementary information, Fig. S3b). The GCaMP6s-SMO-mCherry could induce downstream Hh pathway signaling comparably with SMO(WT) (Supplementary information, Fig. S3c). These results demonstrated that the GCaMP6s-SMO-mCherry was properly folded and behaved like WT SMO. In cells, the GCaMP6s-SMO-mCherry puncta partially colocalized with the early endosome marker early endosome antigen 1 (EEA1) and the recycling endosome marker Transferrin receptor (TfR) (Fig. 2b). Thus, the GCaMP6s-SMO-mCherry reporter primarily tracked the SMO proteins that resided in the endosomal compartments. Strikingly, ShhN treatment substantially increased the luminal  $[\text{Ca}^{2+}]$  of SMO-localized endosomes in NIH3T3 cells (Fig. 2c, d; Supplementary information, Video S1). Knockout of *Ptch1* abrogated the Hh-induced increase of luminal  $[\text{Ca}^{2+}]$  in SMO-localized endosomes (Fig. 2d), suggesting that the  $[\text{Ca}^{2+}]$  elevation was downstream of and dependent on Hh–PTCH1 axis.

To locate the calcium source, we switched the cells into  $\text{Ca}^{2+}$ -free medium and found that ShhN failed to increase the  $[\text{Ca}^{2+}]$  of SMO compartments, which could be restored by the supplement of  $\text{Ca}^{2+}$  (Fig. 2e; Supplementary information, Fig. S3d). Consistently, removal or chelation of extracellular  $\text{Ca}^{2+}$  rendered the cells insensitive to Hh-induced SMO cholesterylation (Fig. 2f). Because  $\text{Ca}^{2+}$  is required for the interaction between Hh and PTCH1 through the globular interface of Hh, we compared the effect of extracellular  $\text{Ca}^{2+}$  on WT Hh and Hh(R153E), a mutant that diminished the  $\text{Ca}^{2+}$ -dominated interface.<sup>24</sup> The result showed that ShhN(R153E) displayed lower potency to induce *Gli1* expression, which could be further inhibited by  $\text{Ca}^{2+}$  removal, indicating that extracellular  $\text{Ca}^{2+}$  is required for downstream signaling besides the Hh–PTCH1 interaction (Fig. 2g). Depletion of extracellular  $\text{Ca}^{2+}$  blunted the interaction of PTCH1 with wildtype



ShhN (Supplementary information, Fig. S3e, f).<sup>24,25</sup> We further examined the effect of lanthanum ( $\text{La}^{3+}$ ) and gadolinium ( $\text{Gd}^{3+}$ ), two trivalent ions known to block cell surface calcium channels.<sup>26–28</sup> Indeed, antagonizing calcium influx with 100  $\mu\text{M}$  of  $\text{La}^{3+}$  and 100  $\mu\text{M}$  of  $\text{Gd}^{3+}$  diminished the calcium elevation in SMO-localized endosomes, cholesterol modification of SMO, as well as Hh

signaling activity (Fig. 2h–k). These data were in line with the in vitro results that SMO cholesterylation and transesterification were boosted by  $\text{Ca}^{2+}$  (Fig. 1c, g). Since SAG directly binds the transmembrane domain of SMO and activates SMO, we indeed observed that the SAG-induced Hh pathway activation was not impaired by extracellular  $\text{Ca}^{2+}$  depletion (Supplementary

**Fig. 2 Hh increases  $[Ca^{2+}]$  in SMO-localized endosomes.** **a** Illustration of a ratiometric SMO-local  $Ca^{2+}$  reporter. **b** Co-localization of GCaMP6s-SMO-mCherry-FLAG reporter with endosome markers EEA1 and TfR in NIH3T3 cells. FLAG was pseudocolored in green whereas Alexa-647-labeled organelle markers were pseudocolored in red. Bar = 10  $\mu$ m. **c** ShhN induced elevation of  $[Ca^{2+}]$  in SMO-localized endosomes. Bar = 10  $\mu$ m. **d** Quantification of ratiometric GCaMP6s intensities upon ShhN treatment in WT and *Ptch1*-KO NIH3T3 cells. **e** Effect of  $[Ca^{2+}]$  in culture media on  $[Ca^{2+}]$  in SMO-localized endosomes. 100 puncta from 10 cells in each condition were analyzed. \*\*\*\* $P < 0.0001$ , two-sample *t*-test. **f** Removal of extracellular  $Ca^{2+}$  inhibited SMO cholesterylation in HEK-293T cells. **g** Expression of *Gli1* mRNA after 8-h incubation with indicated dilution of ShhN conditioned medium in normal (1.8 mM  $Ca^{2+}$ ) or  $Ca^{2+}$ -free media. Inset denoted equal expression of Shh(WT) and Shh(R153E). **h** Representative confocal images of live cells treated with lanthanum chloride and gadolinium chloride (100  $\mu$ M each), in the presence or the absence of ShhN. Bar = 10  $\mu$ m. **i** Quantification of ratiometric GCaMP6s intensities in **h**.  $n = 70, 80$  and  $80$  for each treatment. \*\*\*\* $P < 0.0001$ , two-sample *t*-test. **j** The 100  $\mu$ M of  $La^{3+}$  and  $Gd^{3+}$  attenuated the agonistic effect of ShhN on SMO cholesterylation in cells. **k** Effect of  $La^{3+}$  and  $Gd^{3+}$  on ShhN-induced *Gli1* expression. In **g, k**, data are presented as means  $\pm$  SD. Non-linear fitting was performed in Origin 8 using the built-in DoseResp function.  $P = 6.0363E-8$  (**g**), and  $6.6289E-8$  (**k**). Two-way ANOVA with Tukey's test. In **e** and **i**, boxes denote 25<sup>th</sup> and 75<sup>th</sup> quantiles, while horizontal lines denote median values.

information, Fig. S3g), indicating that the signal transduction downstream of SMO is independent of extracellular  $Ca^{2+}$ . Collectively, these results suggest that Hh-PTCH1 axis stimulates the influx of extracellular  $Ca^{2+}$  to the lumen of SMO-localized endosomes, increases cholesterylation of SMO-CRD and then elicits the downstream signal transduction.

### Hh triggers store-operated calcium entry

In order to search for the calcium channel that contributes to Hh-induced  $Ca^{2+}$  influx, we constructed a mini CRISPR-Cas9 guide RNA (gRNA) library targeting 39 distinct calcium channels and performed a screening in NIH3T3 cells. As SAG-induced Gli-luciferase is independent of  $Ca^{2+}$  influx (Supplementary information, Fig. S3g), the ratio of ShhN-induced Gli-luciferase activity to SAG-induced Gli-luciferase signal was used as the selection readout (Supplementary information, Fig. S4a). Guide sequences were provided in Supplementary information, Table S1. The efficiencies of sgRNAs were validated by T7E1 assay (Supplementary information, Fig. S4b). *Orai1* stood out in the screening, as knockout of *Orai1* resulted in the lowest value of ShhN/SAG-induced Gli-luciferase ratio. To validate this hit, we generated two independent clonal cell lines using gRNA against *Orai1* (Supplementary information, Fig. S4c). Knockout of *Orai1* significantly blocked the ShhN-induced *Gli1* expression (Fig. 3a). The cholesterylation of SMO was also reduced in *Orai1*-knockout cells (Fig. 3b), while overexpression of the dominant-negative mutant of ORAI1(E106Q) reduced SMO cholesterylation in a dose-dependent fashion (Supplementary information, Fig. S4d). Knockdown of other possible candidates, including *Trpm5*, *Trpm6*, *Trpc5* or *P2x1* did not dramatically change the *Gli1* expression or SMO cholesterylation (Supplementary information, Fig. S4e–g). The information for shRNA sequences is provided in Supplementary information, Table S1. However, we cannot completely exclude the possibility that other calcium transporters are involved in the signal transduction downstream of Hh.

It is well-documented that Stromal interaction molecule (STIM) proteins directly interact with ORAI1 to drive  $Ca^{2+}$  refilling.<sup>29,30</sup> Mammalian cells express two STIM proteins, namely STIM1 and STIM2, which respond to the ER  $Ca^{2+}$  depletion to activate  $Ca^{2+}$  release-activated  $Ca^{2+}$  (CRAC) channels including ORAI proteins.<sup>29,31</sup> We then examined the roles of STIM1/2 in SMO cholesterylation and Hh signaling. Knockout of both *Stim1* and *Stim2* abrogated SMO cholesterylation induced by ShhN, as well as downstream GLI1 production (Fig. 3c, d; Supplementary information, Fig. S5a). Similar results were observed in *Stim1/2* double knockdown cells (Supplementary information, Fig. S5b–e). Of note, deletion of *Stim1/2* or *Orai1* significantly decreased the luminal  $[Ca^{2+}]$  of SMO-localized endosomes (Fig. 3e), highlighting the importance of STIM-ORAI1 complex for  $Ca^{2+}$  influx. Since the ER  $Ca^{2+}$  depletion induces STIM1 oligomerization that causes ORAI1 activation,<sup>32</sup> we then used the rapamycin-induced STIM1 oligomerization system to directly activate ORAI1 (Fig. 3f). The  $[Ca^{2+}]$  in SMO-localized endosome was dramatically elevated post

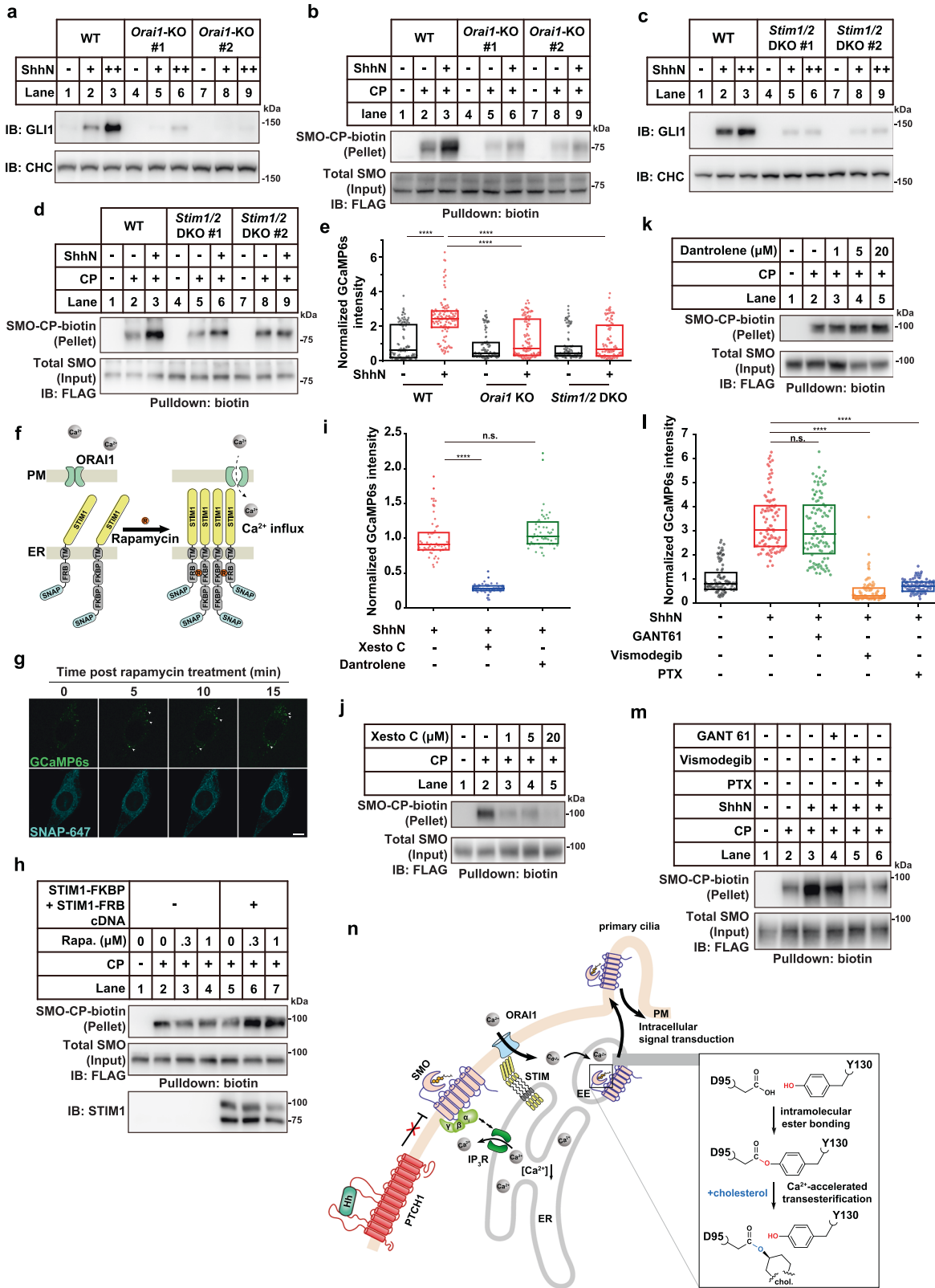
rapamycin treatment (Fig. 3g; Supplementary information, Video S2). Consistently, rapamycin treatment enhanced SMO cholesterylation in the STIM1-FKBP and STIM1-FBP expressing cells, but not in control cells (Fig. 3h).

To examine whether Hh drives the activation of ORAI1 that responds to the depletion of ER  $Ca^{2+}$ , we directly monitored the ER luminal  $[Ca^{2+}]$  using a ratiometric ER calcium sensor named GCEPIA1-SNAP-ER.<sup>33</sup> The result showed that ShhN treatment evoked a global reduction in ER luminal  $[Ca^{2+}]$  (Supplementary information, Fig. S5f). Inositol trisphosphate receptors (IP<sub>3</sub>Rs) and ryanodine receptors (RyRs) are the major ER  $Ca^{2+}$  release channels. Pharmacological inhibition of IP<sub>3</sub>R by xestospongine C significantly reduced the cellular response to ShhN, including the  $[Ca^{2+}]$  elevation of SMO-localized endosomes and SMO cholesterylation (Fig. 3i, j). In contrast, inhibition of RyR by dantrolene had no effect (Fig. 3i–k). These results demonstrate that Hh activates IP<sub>3</sub>R to deplete the ER  $Ca^{2+}$  store.

We next sought to identify upstream modulators of the IP<sub>3</sub>R channels. A previous study has revealed the dependence of Gai-PKA-IP<sub>3</sub>R axis for Hh to induce cytosolic  $Ca^{2+}$  spikes in developing spinal cords in *Xenopus laevis*.<sup>34,35</sup> Interestingly, inhibition of SMO activity by vismodegib or inactivation of Gai by pertussis toxin (PTX) counteracted the Hh-induced  $Ca^{2+}$  elevation in SMO-localized endosomes and SMO cholesterylation, whereas inhibition of GLI transcription factors by GANT 61 showed no distinguishable effects (Fig. 3l, m). These results imply the requirement of SMO-Gai coordination for inducing cellular  $Ca^{2+}$  mobilization. Together, we propose a model of the crosstalk between Hh signaling and  $Ca^{2+}$  dynamics in Fig. 3n. Hh binds PTCH1 and relieves the suppression on SMO. Activation of SMO leads to heterotrimeric G protein assembly,<sup>36,37</sup> which promotes the ER  $Ca^{2+}$  depletion through IP<sub>3</sub>R. The STIM proteins sense the depletion of internal  $Ca^{2+}$  stores and form CRAC channel with ORAI1 to allow extracellular  $Ca^{2+}$  influx, driving the elevation of  $Ca^{2+}$  in SMO-containing endosomal lumen.  $Ca^{2+}$  promotes SMO cholesterylation by catalyzing the ester exchange from D95–Y130 to D95-cholesterol. The cholesterol-modified SMO translocates to primary cilium and amplifies the Hh signaling.

### Cholesterol analogs that bind, but not modify SMO fail to activate Hh signaling

The CRD of SMO is capable of binding a cholesterol molecule as well as being covalently modified.<sup>12–14,38</sup> To distinguish the effects of sterol binding and covalent modification in the CRD, we designed and synthesized cholesterol analogs that were named as C1, C2 and C3 (Fig. 4a). The procedure of chemical synthesis and NMR spectra were presented in Supplementary information, Data S1. C1 and C2 contained a 3-carbonyl and a 3 $\beta$ -amino group, respectively, replacing the 3 $\beta$ -hydroxyl in cholesterol. They bound robustly to the CRD (Fig. 4b–d) and the full-length SMO (Supplementary information, Fig. S6a–c) since these moieties can form H-bonds with D95 carboxyl as 3 $\beta$ -hydroxyl group of cholesterol does. However, the C3 compound with a 3 $\beta$ -



methoxyl failed to bind SMO-CRD (Fig. 4b–d). All these chemical-derived probes were unable to covalently modify SMO, either in vitro or in cultured cells (Fig. 4e; Supplementary information, Fig. S6d). These compounds exhibited efficient cellular uptake when complexed with MβCD (Supplementary information,

Fig. S6e). Notably, none of these analogs was able to drive Hh signaling, as proved by Gli-luciferase reporter, *Gli1* mRNA level, GLI3 processing and SMO ciliary translocation (Fig. 4f–j). As a control, the ciliary localization of 5-hydroxytryptamine subtype 6 receptor (5HT6), a cilia-targeted GPCR,<sup>39</sup> was not affected by any

**Fig. 3** Hh triggers store-operated calcium entry to enhance SMO cholesterylation and drive signal transduction. **a** Immunoblot of GLI1 in *Orai1* knockout NIH3T3 cells. ShhN-conditioned media were used in 1:20 dilution (+) or 1:6 dilution (++). **b** SMO cholesterylation in *Orai1* knockout NIH3T3 cells. **c** Immunoblot of GLI1 in *Stim1* and *Stim2* double knockout (DKO) NIH3T3 cells. ShhN-conditioned media were used in 1:20 dilution (+) or 1:6 dilution (++). **d** SMO cholesterylation in *Stim1* and *Stim2* DKO NIH3T3 cells. **e** Relative ratiometric intensity of GCaMP6s of GCaMP6s-SMO-mCherry reporter in the indicated cells. \*\*\*\* $P < 0.0001$ , two-sample *t*-test. **f** Illustration of rapamycin-inducible STIM1 oligomerization assay. FKBP and FRB bind to rapamycin simultaneously and induce the clustering of STIM1. FKBP, 12-kDa FK502-binding protein; FRB, FKBP-rapamycin-binding domain of mTOR. **g** Confocal live cell imaging of rapamycin-induced GCaMP6s fluorescence increase of GCaMP6s-SMO-mCherry reporter in NIH3T3 cells expressing SNAP-FRB-STIM1 and SNAP-2xFKBP-STIM1. Bar = 15  $\mu\text{m}$ . **h** Rapamycin-induced oligomerization of STIM1 increased SMO cholesterylation. **i** IP<sub>3</sub>R inhibition abrogates Ca<sup>2+</sup> response in SMO-localized endosomes. 10  $\mu\text{M}$  xestospongine C or dantrolene were used to suppress IP<sub>3</sub>Rs or RyRs, respectively.  $n = 50$ . \*\*\*\* $P < 0.0001$ , two-sample *t*-test. **j, k** Effects of IP<sub>3</sub>R or RyR inhibition on SMO cholesterylation. **l** Requirement of SMO-Gai coupling for SMO-localized endosomal Ca<sup>2+</sup> response. Experiments were performed similar to **i**. Vismodegib, 1  $\mu\text{M}$ ; pertussis toxin, 100 ng/mL; GANT 61, 10  $\mu\text{M}$ .  $n = 100$ . \*\*\*\* $P < 0.0001$ , two-sample *t*-test. **m** Gai inhibition impairs Hh-induced enhancement of SMO cholesterylation. **n** Model of the crosstalk between Hh signaling and Ca<sup>2+</sup> dynamics. EE, early endosome. In **e, i** and **l**, boxes denote 25<sup>th</sup> and 75<sup>th</sup> quantiles, and horizontal lines denote median value.

of these compounds (Supplementary information, Fig. S6f, g). Although the CRD binder C1 and C2 showed no detectable pathway activity, they partially antagonized the activation effect of cholesterol, suggesting they competed off cholesterol to engage the CRD (Fig. 4k).

### SMO(D95E) is a loss-of-function mutant that binds cholesterol but is not modified by cholesterol

To further support the notion that SMO-CRD must be covalently modified by cholesterol to exert its signaling activity, we aimed to find a mutant of SMO-CRD which retained the ability to bind cholesterol, but was unable to undergo cholesterylation. Docking simulation suggested that mutation of Asp95 to Glu (D95E) did not interfere with cholesterol binding (Supplementary information, Fig. S7a), which was confirmed by the *in vitro* binding assay (Fig. 5a; Supplementary information, Fig. S7b). Competitive binding assay with <sup>3</sup>H-cholesterol revealed similar affinities of WT and D95E mutant SMO-CRD towards cholesterol (Fig. 5b). Intriguingly, SMO(D95E) was not modified by cholesterol (Fig. 5c), similar to the non-binder SMO(D95N). This result was consistent with the lack of intramolecular ester bond between E95 and Y130 (Supplementary information, Fig. S7c). We then evaluated the function of D95E mutant to transduce Hh signaling. We first compared the ciliary localization efficiency upon ShhN treatment. ShhN induced ciliary localization of SMO (WT) in a time-dependent fashion. On the contrary, SMO(D95E) and SMO(D95N) barely translocated to cilia (Fig. 5d, e). 24(S)-hydroxycholesterol (24S-OHC), a cilia-associated oxysterol, also promoted ciliary localization of SMO(WT), but not the D95 mutants (Fig. 5f). The BODIPY-cyclopamine binding assay<sup>40</sup> showed that these SMO variants robustly bound the fluorescent derivative of cyclopamine (Supplementary information, Fig. S7d). They also translocated to the primary cilia under the stimulation of SAG (Supplementary information, Fig. S7e, f). These results suggest that the mutant SMO proteins fold and traffic to cell surface normally. Cholesterol, 24(S)-hydroxycholesterol and ShhN could dose-dependently activate the GLI-driven luciferase in the presence of SMO(WT) (Fig. 5g–i). However, neither SMO (D95E) nor SMO(D95N) promoted the luciferase reporter activities (Fig. 5g–i).

To validate the function of SMO(D95E) *in vitro*, we generated a D99E knock-in mouse strain (Supplementary information, Fig. S7g). The *Smo*<sup>WT/D99E</sup> heterozygotes were viable and fertile, without obvious abnormalities. However, homozygosity of *Smo*<sup>D99E/D99E</sup> led to severe embryonic developmental defects, as observed in 9.5 days post coitum (dpc) embryos (Fig. 5j). The phenotypes highly resembled that of *Smo*<sup>D99N/D99N</sup> or *Smo*<sup>-/-</sup>,<sup>14,19</sup> demonstrating that the D95E mutation completely abolished SMO function *in vitro*. Cross-sectioning of 9.5 dpc embryo revealed lack of graded expression of Olig2 and Nkx6.1 in neural tubes of homozygotes, which is a hallmark of Hh signal malfunctioning (Fig. 5k). *Smo*<sup>WT/D99E</sup> hybrid cross generated WT

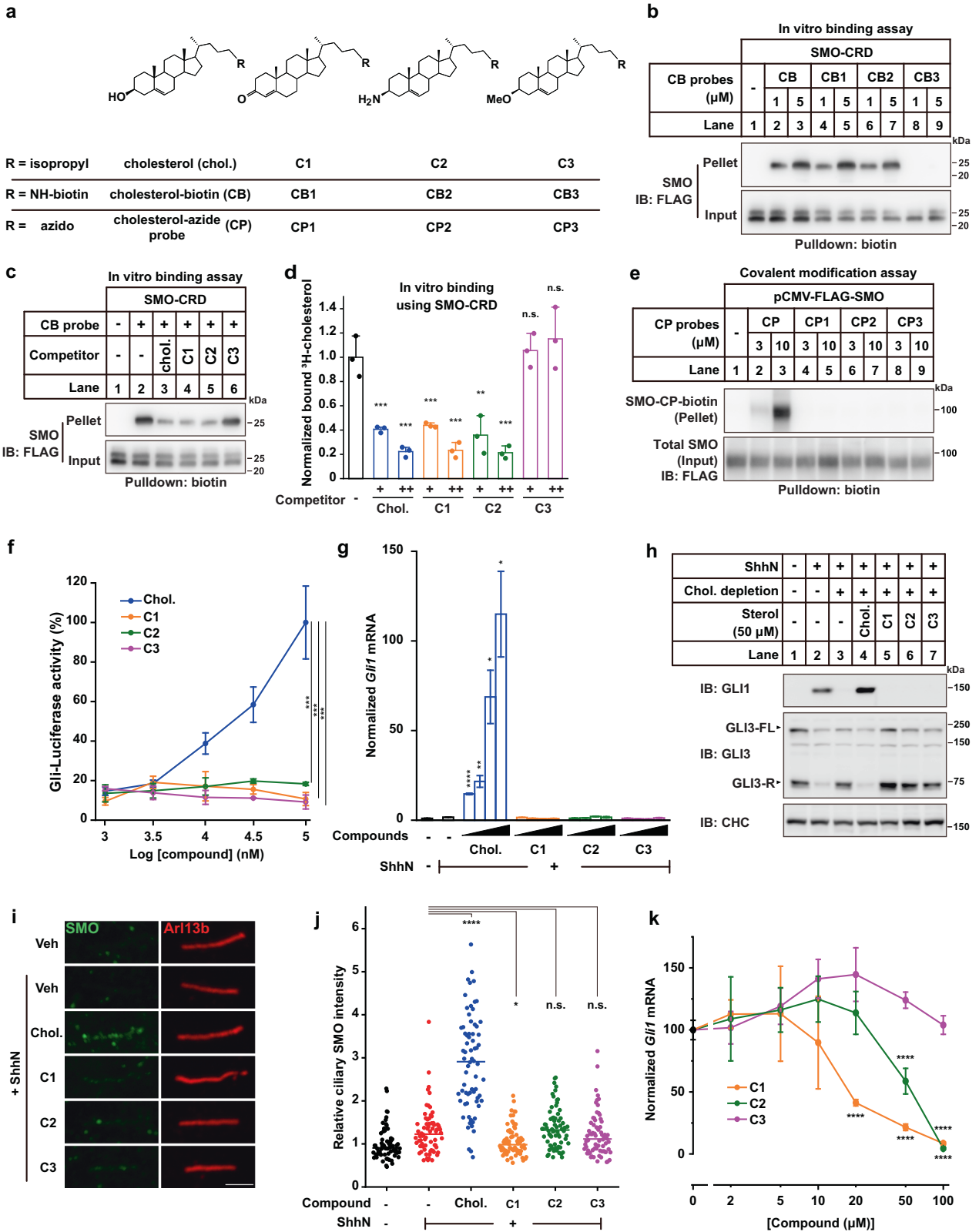
and heterozygote offspring in a ratio of ~1:2, while no homozygote was obtained (Supplementary information, Fig. S7h). Examination of 14.5 dpc embryo revealed a severe developmental delay in homozygotes, as evidenced by unseparated limb digits and faint retina pigmentation (Supplementary information, Fig. S7i). In addition, the homozygous embryos were softer and easily disassembled, suggesting they were likely to be expired. In 17.5 dpc, the homozygous embryos were almost completely absorbed. These data proved that *Smo*<sup>D99E/D99E</sup> is embryonic lethal. The limb development of heterozygotes was normal (Supplementary information, Fig. S7j, k). Therefore, the D95E mutant of SMO with impaired cholesterol modification but normal cholesterol binding, has no activity in Hh signaling.

Together with the data from cholesterol analogs (Fig. 4), we conclude that the cholesterol binding to CRD without covalent modification is insufficient to activate SMO signaling. Instead, cholesterol modification on the D95 of SMO-CRD is required for SMO activation.

### DISCUSSION

Here, we report that the chemistry of SMO autocholesterylation involves a unique two-step mechanism: the formation of a D95–Y130 intramolecular ester bond, followed by the ester exchange from Y130 to cholesterol. This observation is supported by several lines of structural and chemical evidence. First, the close-proximity of D95 carboxyl, Y130 hydroxyl and 3 $\beta$ -hydroxyl of cholesterol, as observed in several studies,<sup>12,38</sup> provides the structural basis. The unique characteristics of the triad ensure specific ester bonding as well as rapid transesterification in the presence of Ca<sup>2+</sup>. We indeed detected the D95–Y130 conjugate by MS/MS. Second, the ester bond between the carboxyl of D95 and phenolic hydroxyl group of Y130 is more active in chemistry. Therefore, it can facilitate the ester exchange with cholesterol. The mechanism that the D95–Y130 ester bond is a prerequisite for cholesterol modification could also explain why SMO(D95E), which lacks intramolecular ester bond, binds cholesterol, but is not subjected to cholesterylation. Structural simulation shows that the distance between the carboxyl group of E95 and the phenolic hydroxyl group of Y130 is 4.8 Å, longer than 2.7 Å for D95 (Supplementary information, Fig. S7a), which precludes the ester bond intermediate formation.

The interplay between calcium signaling and Hh pathway has been suggested. The ER-localized calcium channels, responsible for calcium store release, are activated by Hh in *Xenopus laevis* and zebrafish.<sup>35,41</sup> In addition, it has been reported that the calcium channels on the PM or primary cilium are opened to allow calcium influx in response to Hh stimulation.<sup>42,35</sup> In general, these results are consistent with ours although different species or tissues might use different channels. We here identify IP<sub>3</sub>R, STIM1/2 and ORAI1 are responsible for Ca<sup>2+</sup> mobilization in NIH3T3 cells.



ORAI1-mediated Ca<sup>2+</sup> influx may serve as a general responsive mechanism to Hh, due to the ubiquitous distribution of ORAI1 among different tissues.<sup>43</sup>

Previous studies have emphasized that the activity of SMO is governed by its accessibility to cholesterol on the PM, controlled

by the transporter-like behavior of PTCH1.<sup>15,44,45</sup> In the absence of Hh, only residual SMO presents in the PM and the majority of SMO locates in the intracellular compartments.<sup>46</sup> In the PM, Hh binding to PTCH1 increases the accessibility of the PM-localized SMO to cholesterol by clogging the tunnel inside of PTCH1.<sup>45,47</sup>



**Fig. 4 Cholesterol analogs that bind, but cannot modify SMO, fail to activate Hh signaling.** **a** Chemical structures of cholesterol and its analogs. **b** In vitro binding of the purified FLAG-tagged SMO-CRD protein with CB probes. **c** In vitro binding of the purified FLAG-tagged SMO-CRD protein with CB probe in the presence of competitors. **d** In vitro binding assay of the purified SMO-CRD with  $^3\text{H}$ -cholesterol in the presence of various competitors at the molar ratio of 1:3 (–) or 1:10 (++) . 0.2  $\mu\text{Ci}$   $^3\text{H}$ -cholesterol were added for each sample.  $^{**}P < 0.01$ ,  $^{***}P < 0.001$ , two-sample *t*-test. **e** Analysis of SMO covalent modification by cholesterol and its analogs-derived azido probes. **f** Measurement of Gli-luciferase activities upon different concentrations of compound treatments in NIH3T3 cells stably expressing Gli-promoted firefly luciferase and a constitutively expressed EGFP as the internal control. All cells received saturated ShhN conditioned medium treatment.  $P = 8.25439\text{E}-8$  (Chol. vs C1),  $8.45384\text{E}-8$  (Chol. vs C2), and  $8.22158\text{E}-8$  (Chol. vs C3). Two-way ANOVA with Tukey's test. **g** Measurement of *Gli1* mRNA level by qPCR. Serum-starved NIH3T3 cells were incubated in 1.5% M $\beta$ CD at 37 °C for 30 min, briefly rinsed, and switched in DMEM containing 1  $\mu\text{M}$  lovastatin, indicated compounds and ShhN-conditioned media (1:6 diluted) for 16 h. The compounds were dissolved in M $\beta$ CD as 5 mM stock solutions and the final concentrations of compounds in complex with M $\beta$ CD were 10, 25, 100 and 250  $\mu\text{M}$  in DMEM.  $^{*}P < 0.05$ ,  $^{**}P < 0.01$ ,  $^{***}P < 0.0001$ , two-sample *t*-test, all values were compared to that of column 2. **h** Immunoblot analysis of GLI1 protein upon compounds treatment. NIH3T3 cells were seeded in 60-mm dishes and were treated as described in **g**. **i** Representative confocal images of SMO and primary cilium marker Arl13b after endogenous cholesterol depletion followed by 2-h treatment of indicated compounds in the presence of ShhN. Bar = 2  $\mu\text{m}$ . **j** Quantification of ciliary SMO intensities in **i** ( $n = 60\text{--}70$  cilia for each group). Comparisons were carried with one-way ANOVA with Bonferroni's multiple comparison test. From left to right,  $P < 0.0001$ ;  $P = 0.0108$ ;  $P = 0.3558$ ;  $P = 0.4421$ . **k** Antagonizing effect of the analogs against endogenous cholesterol to induce *Gli1* mRNA expression. NIH3T3 cells were treated with ShhN-conditioned media, along with indicated concentrations of competitive compounds for 16 h and harvested for RNA extraction.  $^{****}P < 0.0001$ , two-sample *t*-test. In **d**, **f**, **g** and **k**, data are presented as means  $\pm$  SD from 3 independent replicates.

Meanwhile, the extracellular free  $[\text{Ca}^{2+}]$  is about 1.2 mM that is sufficient to promote SMO cholesterylation (Fig. 1c).<sup>48</sup> In the SMO-localized endosomes with high level of cholesterol and low level of calcium,<sup>49,50</sup> the luminal  $[\text{Ca}^{2+}]$  becomes a rate-limiting factor. Hh stimulation increases the  $[\text{Ca}^{2+}]$  in endosomal lumen that enhances SMO cholesterylation.

The structural studies revealed multiple sterol binding sites in the TMD and the linker domain of SMO.<sup>16,17</sup> A putative intramolecular tunnel inside SMO stretched from the TMD to the CRD.<sup>16,17</sup> To reconcile these findings, we hypothesize that cholesterol might reach CRD through this tunnel. Cholesterylation of the CRD might induce a conformational change that clog the extracellular exit of the tunnel, thereby stabilizing cholesterol in the TMD and eventually leading to the active conformation of the cytosolic interface of SMO.<sup>16</sup> Hh-stimulated cholesterylation of SMO was independent of the primary cilium structure or the ciliary localization of SMO (Supplementary information, Fig. S8). These results are in line with the previous reports showing that the cholesterol distribution controlled by Hh-PTCH1 can happen in the cilium-free HEK-293 cells.<sup>44,45,51,52</sup> Therefore, our results suggest that the local  $[\text{Ca}^{2+}]$  is another key factor for SMO cholesterylation and activation besides cholesterol accessibility.

In summary, this study reveals the reaction mechanism and demonstrates the biological function of cholesterol conjugation to SMO. It also identifies the coordination between Hh signaling and  $\text{Ca}^{2+}$  dynamics. In addition, this study evokes some key questions that need to be addressed in the future. For instance, how does the cholesterylation of CRD enable the C-terminal tail to be sensed by cytosolic factors, which further facilitate the translocation of SMO from endosomes to the primary cilium?<sup>46,53–55</sup> How is cholesterylation of the ER-localized SMO regulated since the calcium concentration in ER lumen is high and the cholesterol level in ER is low? These questions need further investigation.

## MATERIALS AND METHODS

### Antibodies

The following antibodies were used in this study: mouse mAb anti-FLAG, clone M2 (F3165, Sigma), mouse mAb anti-acetyl Tubulin, clone 6-11B-1 (T6793, Sigma), mouse mAb anti-SMO, clone E5 (Sc-166685, Santa Cruz), mouse mAb anti-GLI1, clone L42B10 (2643, Cell Signaling Technology), mouse mAb anti-CHC, clone 23 (610500, BD Biosciences), rabbit pAb anti-DYKDDDDK (20543-1-AP, Proteintech), rabbit pAb anti-Stim1 (11565-1-AP, Proteintech), rabbit pAb anti-Stim2 (21192-1-AP, Proteintech), rabbit pAb anti-ARL13B (17711-1-AP, Proteintech), mouse mAb anti-EEA1, clone 14 (610457, BD Biosciences), and mouse mAb anti-Transferrin Receptor, clone H68.4 (13-6800, Invitrogen).

### Chemicals

Cholesterol, thapsigargin,  $\text{CuSO}_4$  and sodium ascorbate were from Sigma. Methyl- $\beta$ -cyclodextrin and hydroxypropyl- $\beta$ -cyclodextrin were from CTD. Inc. SAG, dantrolene sodium and GANT61 were from MedChemExpress. TBTA was from Tokyo Chemical Industry. Rapamycin and vismodegib were from TopScience Biochem. Pertussis toxin and xestospongins C were from Calbiochem. BODIPY-cyclopamine was from Toronto Research Chemicals.

### Cell culture

HEK-293T cells were cultured in Dulbecco's Modified Eagle Medium (DMEM, Thermo Fisher Scientific) plus 10% fetal bovine serum (FBS, Gibco) with pen/strep. NIH3T3 cells and derivatives were cultured in DMEM plus 10% fetal calf serum (FCS, ExcellBio) with pen/strep. All cells were maintained in a humidified chamber with 5%  $\text{CO}_2$ .

### Cloning

pCMV-FLAG-SMO was generated by inserting human *Smo* cDNA into pcDNA3, followed by inserting a 3 $\times$  FLAG epitope-coding DNA after the signal peptide of SMO. The sequence after 1–192 amino acids (a.a.) was truncated to generate pCMV-FLAG-CRD. pCMV-GCaMP6s-SMO-mCherry-FLAG was generated as follows: the signal peptide of Calreticulin was fused to the 5' end of GCaMP6s and amplified by PCR. The SMO-mCherry-FLAG fragment, which contains the coding region of SMO from 34–787 a.a., was amplified from pmCherry-N1-SMO, and attached with a FLAG epitope by PCR. The two fragments were ligated to pcDNA3 vector to generate pCMV-GCaMP6s-SMO-mCherry-FLAG. To generate pCMV-SNAP-2 $\times$ FKBP-STIM1 or pCMV-SNAP-FRB-STIM1, a SNAP-coding cDNA was first amplified from pAAV-GCEPIA-SNAP-ER, and the signal peptide of STIM1 (1–23 a.a.) was fused to the 5' end. The pLenti-OC-IRES-BSD plasmid was kindly provided by Dr. Wen-Sheng Wei (Peking University) and the peGFP-STIM1 was kindly provided by Dr. Jen Liou (UT Southwestern Medical Center). The cDNA sequence encoding STIM1 (208–686 a.a.) was also amplified. The tandem FKBP- or FRB-coding sequences were synthesized, each flanked by two short GS linkers, and were ligated into pcDNA3 vector to generate pCMV-SNAP-2 $\times$ FKBP-STIM1 or pCMV-SNAP-FRB-STIM1. pCMV-HA-ORAI1 was generated by ligating human *Orai1* cDNA into pcDNA3-N-3 $\times$ HA vector, in-frame with the N-terminal HA sequence. All mutations were generated with Agilent QuikChange method. pAAV-GCEPIA-SNAP-ER was a generous gift from Dr. Ping-Yong Xu (Institute of Biophysics, Chinese Academy of Science).

### Molecular docking simulations

Molecular docking studies were carried out using Molecular Operating Environment (MOE 2015.10, Chemical Computing Group, Canada) software. Structure of human SMO protein complex with Cholesterol (PDB accession code: 5L7D) was used for docking. The structure protonation, partial charges and energy minimization of the SMO structure was processed by MOE 2015.10. To docking cholesterol to SMO D95E mutant, the SMO protein amino acid at position 95 was mutated from Aspartic acid (D) to Glutamic acid (E) by Coot software. The next process was carried out

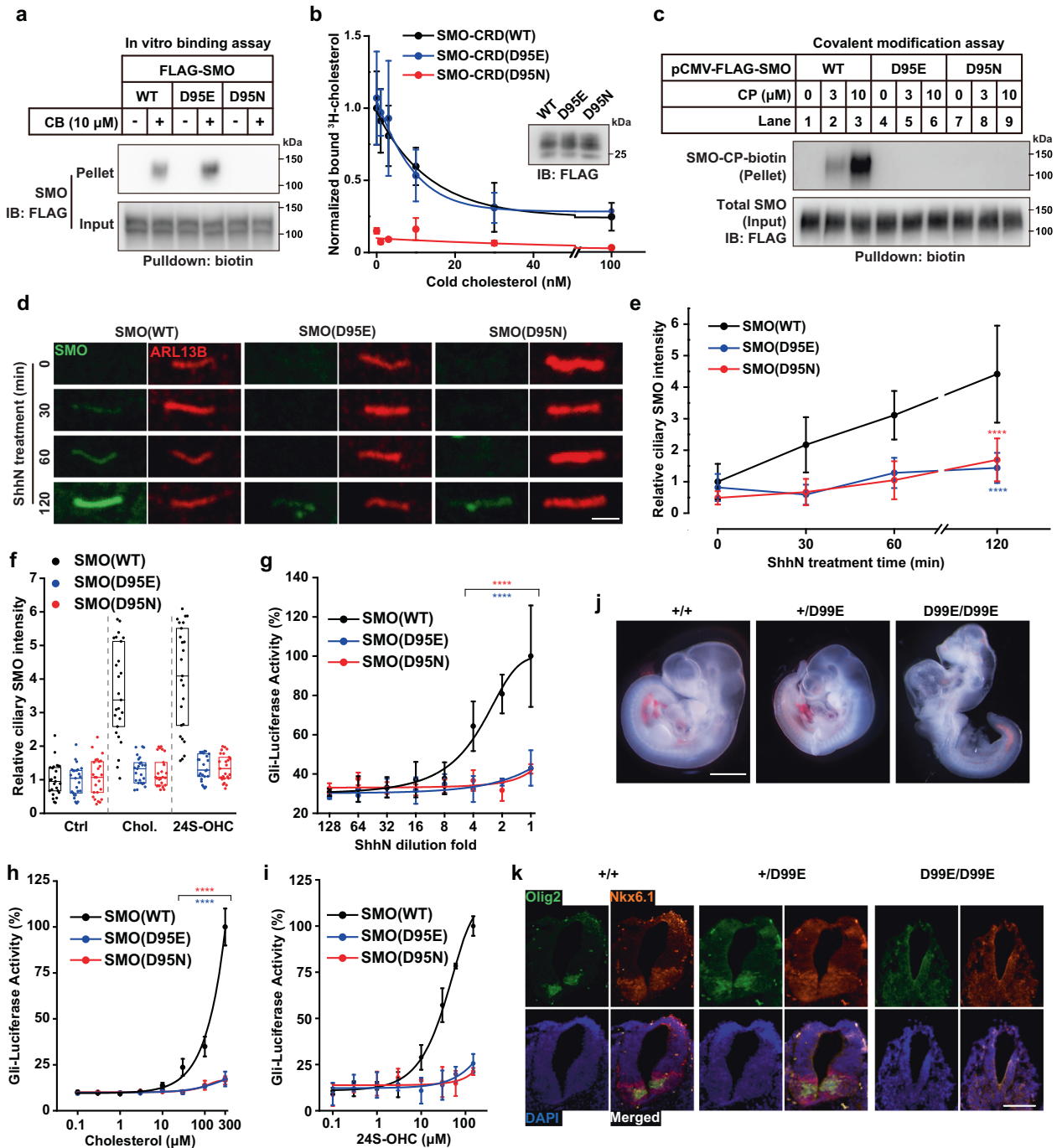


**Fig. 5 SMO(D95E) is a loss-of-function mutant that binds cholesterol but cannot be modified by cholesterol.** **a** In vitro binding assay of the FLAG-tagged SMO variants with CB. **b** In vitro binding assay of the SMO-CRD variants with  $^3$ H-cholesterol in the presence of cold cholesterol as competitors. **c** Analysis of covalent modification of SMO variants by cholesterol-derived CP probe in HEK-293T cells. **d** Representative confocal images of SMO variants on primary cilia upon ShhN ligand treatment in NIH3T3 cells. Bar = 2  $\mu$ m. **e** Quantification of ciliary SMO intensity in **d** ( $n = 20$  cilia in each condition). Comparisons were carried with one-way ANOVA with Bonferroni's multiple comparison test.  $P = 1.050E-7$  (WT vs D95E),  $P = 2.435E-6$  (WT vs D95N). **f** Quantification of ciliary SMO intensity upon 2 h of 100  $\mu$ M of cholesterol or 30  $\mu$ M of 24S-OHC treatment.  $n = 20$ . **g-i** Measurement of Gli-Luciferase activities of SMO variants in response to ShhN ligand (**g**), cholesterol (**h**) and 24S-OHC (**i**) in NIH3T3-Smo-null cells. In **g**,  $P = 2.9602E-7$  (WT vs D95E) and  $1.2687E-7$  (WT vs D95N). In **h**,  $P = 1.8857E-7$  (WT vs D95E) and  $1.2798E-7$  (WT vs D95E). Two-way ANOVA with Tukey's test. **j** Morphologies of mouse embryos of indicated genotypes at 9.5 dpc. **k** Expression of Olig2 and Nkx6.1 in neural tubes of 9.5 dpc embryos. Bar = 0.5 mm. In **b**, **e**, **g**, **h** and **i**, data are presented as means  $\pm$  SD from 3 independent replicates. Non-linear fitting was performed in Origin 8 with the DoseResp function.

as we described above. The first docking was carried out using the Alpha Triangle placement method with London dG scoring. Then the induced fit methods were used to refine the model with GBVI/WASA dG scoring. Finally, the docking structure of the complex with the lowest S-score was selected for further analysis.

#### Immunoblotting

Cells grown on petri dishes were scrapped and collected by centrifugation at 1000 $\times$  g for 5 min. Cells were washed once in phosphate-buffered saline (PBS) and resuspended in 100  $\mu$ L RIPA buffer (50 mM Tris-HCl pH 8.0, 150 mM NaCl, 0.1% SDS, 1.5% NP40 and 0.5% deoxycholate) containing

protease inhibitors (1 mM PMSF, 5 µg/mL pepstatin A, 10 µg/mL leupeptin, 25 µg/mL acetyl-leucyl-leucyl-norleucinal and 10 µM MG132) and incubated on ice for 30 min. Lysates were centrifuged at 13,000×g for 10 min at 4 °C and pellets were discarded.

For soluble protein blotting, samples were mixed with 1/3 volume of 4× reducing sample buffer (1 M Tris-HCl, pH 6.8, 6% β-mercaptoethanol, 12% SDS, 30% glycerol and 0.1% bromophenol blue) and boiled at 95 °C for 5 min. For SMO blotting, samples were mixed with equal volume of solubilization buffer (62.5 mM Tris-HCl, pH 6.8, 15% SDS, 8 M urea, 10% glycerol and 100 mM dithiothreitol) and incubated at 37 °C for 30 min, and then mixed with 2/3 volume of 4× reducing sample buffer before loading on gel. Resolved proteins on SDS-PAGE were then transferred onto 0.45 µm pore size PVDF membrane (Immobilon-P, Millipore). Membranes were blocked with 5% non-fat dry milk in TBS-T, incubated with primary and secondary antibodies, and visualized with Pierce ECL Pico or Femto substrates (Thermo Fisher Scientific).

### Immunofluorescence

Cells grown on coverslips were fixed with 4% paraformaldehyde at room temperature for 20 min. Coverslips were washed with PBS, permeabilized with 0.1% Triton X-100, and blocked with 2% bovine serum albumin (BSA) in PBS. Cells were then stained with primary antibody diluted in BSA/PBS solution overnight at 4 °C. For staining of SMO, anti-SMO antibody was first diluted and incubated with fixed and permeabilized *Smo*-null NIH3T3 cell pellet overnight to reduce non-specific signal. Cell pellets were centrifuged and discarded, and supernatant was used for immunostaining of SMO. Fluorophore-conjugated secondary antibody was also diluted 1:1000 in BSA/PBS and applied to coverslips for 1 h at room temperature. Coverslips were mounted with FluorSave mounting medium (Millipore) and images were captured with an SP8 confocal microscope (Leica) equipped with a HyD detector.

Image quantification was performed using Fiji. SMO channel was thresholded and masked by the cilium marker (Arl13b) channel, and then the fluorescence intensities in the region were quantified, normalized, and plotted.

Live-cell imaging for recoding GCaMP6s signal was conducted in NIH3T3 cells stably expressing GCaMP6s-SMO-mCherry reporter. Cells were seeded in glass-bottom dishes and serum-starved overnight. The culture dish was placed in a pre-warmed chamber on the 63× objective. The images from 5 µm of z-axis, which was comprised of 12 optical sections were captured. Maximum projection images were generated and analyzed. For the quantification of GCaMP6s signal intensities, 10 puncta were randomly chosen from each cell. The ratio of  $f_{\text{GCaMP6s}}$  and  $f_{\text{mCherry}}$  in each punctum was quantified in Leica LAS AF software and plotted.

### Luciferase assay

For the analysis of endogenous SMO, NIH3T3 reporter cells were plated in 24-well plates and allowed to reach confluence. Cells were then incubated in DMEM plus 0.5% FCS overnight, switched to DMEM containing 1.5% hydroxypropyl-β-cyclodextrin for 15 min, briefly washed and incubated in DMEM containing 1 µM lovastatin, ShhN conditioned medium and compounds as indicated.

For SMO variants analysis, *Smo*-null NIH3T3 cells were plated in 24-well plates and each well was transfected with 0.15 µg *Smo* cDNA, 0.15 µg DNA encoding GliBS-firefly luciferase and additional 0.05 µg pEGFP-N1 as an internal control. Transfections were performed with Lipofectamine 2000. Cells were subsequently treated as described in DMEM plus 0.5% FCS for 36 h.

### RNA expression analysis

NIH3T3 cells in 60 mm petri dishes were treated as described. Total RNA was isolated using TRIzol (Thermo Fisher Scientific). 2 µg of total RNA was used for reverse transcription with oligo dT. Quantitative PCR (qPCR) was conducted using Hieff qPCR SYBR Green master mix (Yeasen Biotech). The following primers were used: mGli1-F TACTCGGGGTTCAATGATGC, mGli1-R TGTGGAGTTGGGGCTAGACAT, mGapdh-F TGGCTTCCTGTTCTCTAC and mGapdh-R GAGTTGCTGTTGAAGTCGCA.

### Covalent cholesterol modification assay of SMO in cultured cells

Covalent modification assay was carried out as previously described.<sup>14</sup> HEK-293T cells grown in 10 cm petri dishes were transfected with 6 µg *Smo* cDNA and 15 µg linear polyethylenimine. The second day after transfection, cells

were incubated in DMEM/10% FBS plus indicated concentration of CP probe for 16 h. Cells were lysed in RIPA buffer and lysates were clicked with alkyne biotin. The reaction mixture was dialyzed twice and pulled down with NeutrAvidin agarose (Thermo Fisher Scientific). Beads were extensively washed, and bound proteins were eluted by boiling beads in 2× loading buffer. The supernatant was then aspirated, mixed with equal volume of solubilization buffer and subjected to immunoblotting.

### In vitro binding assay of SMO

For analysis of SMO binding to CB probes, SMO protein, which was immunocaptured with M2 anti-FLAG beads (Sigma) as previously described,<sup>14</sup> was incubated with 10 µg/mL CB probe dissolved in binding buffer (20 mM HEPES, pH 7.4, 150 mM NaCl, and 0.2% DDM) at 4 °C for 4 h. The beads were washed three times with binding buffer, and protein complex was eluted in 400 µL of binding buffer plus 0.1 mg/mL FLAG-peptide before mixed with NeutrAvidin beads. The beads and bound protein were processed as described in the previous section.

For binding assay of SMO-CRD protein to <sup>3</sup>H-cholesterol, FLAG-tagged SMO-CRD protein was purified from HEK-293T cell and immobilized on beads. Briefly, HEK-293T cells transfected with pCMV-FLAG-SMO-CRD were lysed in lysis buffer (20 mM Tris-HCl, pH 7.4, 150 mM NaCl, and 1% Triton-X 100) with protease inhibitors. Clarified lysates were incubated with M2 anti-FLAG beads at 4 °C with end-over-end rotation for 4 h. Beads were extensively washed with TKN buffer (20 mM Tris-HCl, pH 7.4, 50 mM KCl, 0.001% NP-40) and aliquoted. Radioactive cholesterol (in ethanol stock) was diluted 1:250 in TKN buffer and vigorously vortexed at room temperature for 4 h, giving rise to ~200 nM cholesterol solution and then aliquoted to 500 µL per sample. Competitors were added and shaken to homogeneity. The mixture was then added to the protein-bound beads and incubated overnight at 4 °C with end-over-end rotation. Beads were then washed thrice with TKN buffer, and bound proteins were eluted in TKN buffer plus 0.1 mg/mL FLAG-peptide. Eluted protein complexes were mixed with 5 mL liquid scintillation cocktail (Optiphase HiSafe, Perkin Elmer) and shaken to homogeneity. The radioactivity was then measured by a scintillation counter (Tri-Carb 2910TR, Perkin Elmer). A control using mock-transfected cell was included, and the CPM value was subtracted from all samples as a background.

### In vitro cholesterol modification assay of SMO

The FLAG-tagged SMO or SMO-CRD protein was immunopurified with anti-FLAG beads and eluted with FLAG peptide in 20 mM HEPES, pH 7.4, 150 mM NaCl plus 0.2% DDM. Approximately 5 µg FLAG-tagged SMO-CRD or 1 µg FLAG-tagged full-length SMO protein was incubated with 10 µM (or indicated concentrations) CP probe diluted in 500 µL buffer and subjected to shaking for indicated time (Fig. 1b) or 30 min at 37 °C in dark. The indicated divalent ion salts were also added. The mixture was then centrifuged at 13,200×g for 10 min at 4 °C. The supernatant was aspirated and dialyzed for 2 h against RIPA and subjected to click chemistry, the following procedures were identical to previously described.

### Mass spectrometry sample preparation

The purification of CRD was carried out as previously described. For the comparison of ester bond ratio in Supplementary information, Fig. S2e, 2 mM EDTA was included in the lysis and binding buffer throughout the procedure. The protein was eluted in TBS (20 mM Tris-HCl, pH 7.6 plus 150 mM NaCl) buffer with or without 2 mM CaCl<sub>2</sub>, incubated at 37 °C for 30 min, and immediately subjected to protease digestion. The purified CRD protein in TBS was firstly supplemented with trypsin (Promega) to a final concentration of 10 ng/µL and digested for 12 h at 37 °C. Elastase (Promega) was then added to final concentration of 10 ng/µL and the mix was incubated for 1 h at 37 °C. The digested peptides were desalted in a house-made C18 stage-tip and dried in a vacuum centrifuge.

### LC-MS/MS analysis

Desalted peptides were resuspended in Solvent A (0.1% formic acid) and separated on a homemade C18 column<sup>56</sup> (3 µm, 120 Å Uchrom C18, nanoLCMS Solutions; 75 µm × 20 cm) at a flow rate of 250 nL/min using a 60 min gradient of 2%–35% Solvent B (0.1% formic acid, 100% acetonitrile). Easy-nanoLC was coupled to a Q Exactive HF mass spectrometer (Thermo Scientific, San Jose, CA). For data-dependent acquisition (DDA), full-scans (m/z 100–1200) were acquired in the orbitrap with a resolution of 60,000 at m/z 200, and the 20 most abundant ions in each MS scan were

automatically selected and fragmented in HCD mode at a resolution of 30,000. Normalized collision energy (NCE) was set to 27.

For the analysis of cellular compound uptake, cells in 60-mm dishes were treated with indicated compounds, washed with ice-cold DPBS twice, and harvested by scraping. 200  $\mu$ L ethanol was added to cell pellets, and the mixture was sonicated for 10 min on ice. The samples were then snap-frozen in liquid nitrogen, thawed, and sonicated thrice. 1 mL of hexane were added to each tube and sonicated for 10 min. The samples were centrifuged at 16,000 $\times$  *g* for 10 min. The upper organic layer was collected to a new centrifuge tube and was vacuum dried. The remnants were used for protein quantification. The lipids were resuspended in 35  $\mu$ L of isopropanol and analyzed by ultraperformance liquid chromatography with tandem mass spectrometry (UPLC-MS/MS) conducted on a Waters Acquity UPLC-system coupled with 5500 QTRAP system (SCIEX). Chromatographic separation was achieved on a Waters Acquity UPLC BEH C18 Column (2.1 mm  $\times$  100 mm, 1.7  $\mu$ m particles) using a flow rate of 0.4 mL/min at 55  $^{\circ}$ C during a 10 min gradient (0–2 min from 50% B to 95% B, 2–3 min from 95% B to 98% B, 3–8 min 98% B, 8–9 min from 98% B to 50% B, 9–10 min 50% B), using solvent A (60:40 water:acetonitrile with 10 mM ammonium formate and 0.1% formic acid) and solvent B (90:10 isopropanol:acetonitrile, with 10 mM ammonium formate and 0.1% formic acid).

Mass spectrometer was installed with an APCI source which was set in positive mode with following the parameters, Curtain Gas 40 psi; Nebulizer Current 3.0 mA; Source Temperature 400  $^{\circ}$ C; Ion Source Gas1 50 psi. The analytes were monitored in multiple reaction monitoring (MRM) mode using the precursor-to-product ion transitions of *m/z* 369.2  $\rightarrow$  147.0 for Cholesterol, *m/z* 368.2  $\rightarrow$  368.2 for CP, *m/z* 385.1  $\rightarrow$  109.0 for C1, *m/z* 383.1  $\rightarrow$  383.1 for C2, *m/z* 386.1  $\rightarrow$  369.3 for C3 and 376.1  $\rightarrow$  376.1 for D7-Cholesterol. Peak determination and area integration were performed using Analyst 1.7.1 (SCIEX) and SCIEX OS1.4.0 software (SCIEX).

The residual precipitants after lipid extraction were washed once with 95% ethanol containing 0.3 M guanidine hydrochloride. The precipitants were briefly dried at 50  $^{\circ}$ C and were resuspended in 200  $\mu$ L of 8 M urea by overnight vortexing. Protein quantification was performed with BCA assay using bovine serum albumin as standards.

### Database searching

The raw data were processed by Proteome Discoverer (Thermo Scientific, Version 2.1) and searched against the SMO-CRD amino acid sequence. No enzyme (unspecific cleavage) was chosen due to the non-specificity of elastase. Variable modifications included were oxidation on methionine, YMPK (519.25154 Da) and VYMPK (618.31996 Da) on aspartate, DS (202.05897 Da) and GDS (259.08044 Da) on tyrosine. No fixed modification was included. The precursor mass tolerance was set to 10 ppm, and the fragment mass tolerance was set to 0.02 Da. High confidence peptides were used for peptide identification with a false discovery rate (FDR) less than 0.01.

### Flow cytometry-based analysis of BODIPY-cyclopamine binding to SMO

BODIPY-cyclopamine binding assay was carried out essentially as previously described.<sup>12</sup> HEK-293T cells expressing SMO variants were plated in 6-well plates. Cells were washed with PBS once and incubated with BODIPY-cyclopamine (Toronto Research Chemicals) diluted in phenol red-free DMEM, and incubated on ice for 1 h. Cells were then detached with PBS plus 5 mM EDTA and washed with cold PBS for four times. Bound BODIPY intensities were quantified with a flow cytometer (CytoFLEX, Beckman).

### Arrayed screening of plasma membrane Ca<sup>2+</sup> channels responsible for Hh signaling

Lentivirus expressing OCT1-Cas9 was produced in HEK-293T cells by co-transfecting pLenti-OC-IRES-BSD, pSPAX and pMD2.G plasmid.<sup>57</sup> Viral supernatants were collected, centrifuged at 2000 $\times$  *g* for 5 min to remove cell debris, and stored in  $-80^{\circ}$ C until use. Viral supernatant was mixed with fresh medium and supplemented with 8  $\mu$ g/mL polybrene to transduce NIH3T3/Gli-luciferase/EGFP cell to generate Cas9-stably expressing NIH3T3-GCE cell. Cells were screened and maintained in the presence of 5  $\mu$ g/mL blasticidin.

The sequences of sgRNA targeting plasma membrane Ca<sup>2+</sup> channels were extracted from the Brie mouse sgRNA library.<sup>58</sup> Three sgRNA against each gene were selected and synthesized as oligonucleotides

with overhangs to generate sticky ends. The oligonucleotides were annealed and ligated into pLenti-guide-puro. sgRNA-containing lentiviral particles were produced in HEK-293T. Three sgRNAs targeting a single gene were pooled and used to infect NIH3T3-GCE cell. Transduced cells were selected in 2  $\mu$ g/mL puromycin, seeded in 24-well plates and grown to sub-confluency. Cells were then switched into 0.5% FCS/DMEM media. After overnight serum starvation, cells were treated with or without 100 nM SAG or 1:6 ShhN-conditioned medium for 36 h and harvested for luciferase activity measurement with EGFP fluorescence as the internal control.

### Analysis of Ca<sup>2+</sup> level in the ER by flow cytometry

NIH3T3 cells stably expressing GCEPIA-SNAP-ER were plated in 60-mm dishes. After reaching sub-confluency, cells were switched into DMEM containing 0.5% FCS overnight. Then cells received ShhN-conditioned media at 1:6 dilution for 30 min, or 1  $\mu$ M thapsigargin for 5 min at 37  $^{\circ}$ C in Ca<sup>2+</sup>-free media. The cells were then trypsinized and immediately analyzed on a flow cytometer with FITC and APC channels. Relative Ca<sup>2+</sup> level in the ER was calculated by dividing GCEPIA fluorescence by SNAP fluorescence ( $f_{\text{GCEPIA}}/f_{\text{SNAP}}$ ).

### Embryo sectioning and immunostaining

Pregnant female mice on the designated day after vaginal plug were sacrificed by cervical dislocation. Embryos were dissected under a stereo microscope. Embryos were then placed on glass slide with a drop of PBS containing 2 mM EDTA to bleed umbilical blood. Morphological pictures were captured under Olympus SZX16 equipped with a CCD. The embryos were then fixed in 4% paraformaldehyde for 1 h at room temperature. The embryos were washed thrice with PBS and embedded in a drop of PBS plus 2% low-gelling temperature agarose and 2.5% gelatin. After solidification of the solution, the gel block was trimmed and placed in HistoCore Pearl automated tissue processor.

Wax block was sectioned with a HistoCore Biocut microtome with 8  $\mu$ m thickness. Sections were deparaffinized in xylene and ethanol gradient. Antigen retrieval was performed by boiling sections in sodium citrate solution. Sections were then stained with anti-Olig2 and anti-Nkx6.1, followed by fluorophore-conjugated secondary antibodies and inspected under an inverted microscope.

Cartilage and bone staining was performed according to the previous method.<sup>59</sup>

### Quantum mechanical calculation

Two model molecules were built based on the crystal structure of SMO in complex with cholesterol (PDB id: 5L7D) to mimic the intramolecular ester bond between D95 and Y130 (see Supplementary information, Fig. S2), and the ester bond between D95 and cholesterol after covalent modification, respectively. The structures of these two model molecules were optimized first at the M06-2X/6-31 G\* level.<sup>60</sup> The optimized structures were used for calculations of the bonding energies of the ester bonds. To obtain the bonding energy, the single point energy of the complex ( $E(\text{A-B})$ ) was calculated at the M06-2X/6-311 + G\* level. The complex was then decomposed into two free radicals (A $\cdot$  and  $\cdot$ B) by cutting the corresponding ester bond, and their energies ( $E(\text{A}\cdot)$  and  $E(\cdot\text{B})$ ) were also calculated using M06-2X/6-311 + G\*. The bonding energy ( $E_{\text{bond}}$ ) was obtained by  $E_{\text{bond}} = E(\text{A-B}) - E(\text{A}\cdot) - E(\cdot\text{B})$ . All quantum mechanical calculations were carried out using the Gaussian16 program.<sup>61</sup>

### CaCl<sub>2</sub>-catalyzed synthesis of cholesteryl acetate from cholesterol and *p*-tolyl acetate

A mixture of cholesterol (2 g, 5.18 mmol), CaCl<sub>2</sub> (0.57 g, 5.18 mmol) and DMF (10 mL) was mixed with *p*-tolyl acetate (1.56 g, 10.36 mmol). After being stirred at 37  $^{\circ}$ C for 120 h, the residue was poured into H<sub>2</sub>O and extracted with DCM (3  $\times$  60 mL). The combined organic layers were washed with brine, followed by drying over Na<sub>2</sub>SO<sub>4</sub> and concentrated under reduced pressure to afford the yellow solid. Then the solid mixture was purified by silica gel column chromatography (eluent: PE/EtOAc = 80:1) to afford cholesteryl acetate as a white solid (460 mg, 21%). <sup>1</sup>H NMR (600 MHz, CDCl<sub>3</sub>)  $\delta$  5.40 (d, *J* = 5.1 Hz, 1H), 4.66 – 4.58 (m, 1H), 2.34 (d, *J* = 6.7 Hz, 2H), 2.05 (d, *J* = 1.1 Hz, 3H), 2.04 – 1.95 (m, 2H), 1.87–1.89 (m, 3H), 1.54 – 1.40 (m, 4H), 1.43 – 1.33 (m, 4H), 1.32 – 1.26 (m, 4H), 1.20 – 1.09 (m, 6H), 1.06 – 0.96 (m, 6H), 0.94 (d, *J* = 6.5 Hz, 3H), 0.89 (dd, *J* = 6.9, 2.7 Hz, 6H), 0.70 (s, 3H). <sup>13</sup>C NMR (151 MHz, CDCl<sub>3</sub>)  $\delta$  170.60, 139.68, 122.68, 74.01, 56.70, 56.14, 50.04, 42.32, 39.74, 39.53, 38.13, 37.00, 36.60, 36.19, 35.80, 31.91, 31.87, 28.24, 28.03, 27.78, 24.29, 23.83,

22.83, 22.57, 21.46, 21.03, 19.32, 18.72, 11.86. HRMS(ESI): calcd for  $C_{29}H_{48}NaO_2 [M + Na]^+$  451.3547, found 451.3553.

The control experiment was carried out without  $CaCl_2$ . A mixture of cholesterol (2 g, 5.18 mmol) and DMF (10 mL) was added with *p*-tolyl acetate (1.56 g, 10.36 mmol). After being stirred at 37 °C for 120 h, the cholesteryl acetate was not detected by thin-layer chromatography

### Chemical synthesis

The schemes of synthesis of sterol compounds are illustrated in Supplementary information, Data S1.

### REFERENCES

- Vorechovsky, I. et al. Somatic mutations in the human homologue of *Drosophila* patched in primitive neuroectodermal tumours. *Oncogene* **15**, 361–366 (1997).
- Bale, A. E. Hedgehog signaling and human disease. *Ann. Rev. Genom. Human Genet.* **3**, 47–65 (2002).
- Reifenberger, J. et al. Somatic mutations in the *PTCH*, *SMO*, *SUFU* and *TP53* genes in sporadic basal cell carcinomas. *Br. J. Dermatol.* **152**, 43–51 (2005).
- Hu, A. & Song, B. L. The interplay of Patched, Smoothed and cholesterol in Hedgehog signaling. *Curr. Opin. Cell Biol.* **61**, 31–38 (2019).
- Cong, Q., Xu, R. & Yang, Y. Galphas signaling in skeletal development, homeostasis and diseases. *Curr. Top. Dev. Biol.* **133**, 281–307 (2019).
- Ruiz i Altaba, A. Combinatorial *Gli* gene function in floor plate and neuronal inductions by Sonic Hedgehog. *Development* **125**, 2203–2212 (1998).
- Corbit, K. C. et al. Vertebrate Smoothed functions at the primary cilium. *Nature* **437**, 1018–1021 (2005).
- Huangfu, D. et al. Hedgehog signalling in the mouse requires intraflagellar transport proteins. *Nature* **426**, 83–87 (2003).
- Porter, J. A., Young, K. E. & Beachy, P. A. Cholesterol modification of Hedgehog signaling proteins in animal development. *Science* **274**, 255–259 (1996).
- Creanga, A. et al. Scube/You activity mediates release of dually lipid-modified Hedgehog signal in soluble form. *Genes Dev.* **26**, 1312–1325 (2012).
- Tukachinsky, H., Kuzmickas, R. P., Jao, C. Y., Liu, J. & Salic, A. Dispatched and scube mediate the efficient secretion of the cholesterol-modified Hedgehog ligand. *Cell Rep.* **2**, 308–320 (2012).
- Huang, P. et al. Cellular cholesterol directly activates Smoothed in hedgehog signaling. *Cell* **166**, 1176–1187. e14 (2016).
- Luchetti, G. et al. Cholesterol activates the G-protein coupled receptor Smoothed to promote Hedgehog signaling. *eLife* **5**, e20304 (2016).
- Xiao, X. et al. Cholesterol modification of Smoothed is required for Hedgehog signaling. *Mol. Cell* **66**, 154–162. e10 (2017).
- Kinnebrew, M. et al. Cholesterol accessibility at the ciliary membrane controls Hedgehog signaling. *Elife* **8**, e50051 (2019).
- Deshpande, I. et al. Smoothed stimulation by membrane sterols drives Hedgehog pathway activity. *Nature* **571**, 284–288 (2019).
- Qi, X., Friedberg, L., De Bose-Boyd, R., Long, T. & Li, X. Sterols in an intramolecular channel of Smoothed mediate Hedgehog signaling. *Nat. Chem. Biol.* **16**, 1368–1375 (2020).
- Hu, A., Zhou, M. & Song, B. L. Analysis of protein cholesterylation by biorthogonal labeling. *Methods Mol. Biol.* **2374**, 27–36 (2022).
- Zhang, X. M., Ramalho-Santos, M. & McMahon, A. P. Smoothed mutants reveal redundant roles for *Shh* and *Ihh* signaling including regulation of L/R asymmetry by the mouse node. *Cell* **105**, 781–792 (2001).
- Qiu, Z. P., Hu, A. & Song, B. L. The 3- $\beta$ -hydroxysteroid-Delta(8), Delta(7)-isomerase *EBP* inhibits cholesterylation of Smoothed. *Biochim. Biophys. Acta. Mol. Cell Biol. Lipids* **1866**, 159041 (2021).
- Bygrave, F. L. & Benedetti, A. What is the concentration of calcium ions in the endoplasmic reticulum? *Cell Calcium* **19**, 547–551 (1996).
- Luo, J., Yang, H. & Song, B. L. Mechanisms and regulation of cholesterol homeostasis. *Nat. Rev. Mol. Cell Biol.* **21**, 225–245 (2020).
- Guan, C. et al. Structural insights into the inhibition mechanism of human sterol *O*-acyltransferase 1 by a competitive inhibitor. *Nat. Commun.* **11**, 2478 (2020).
- Qi, X., Schmiede, P., Coutavas, E. & Li, X. Two Patched molecules engage distinct sites on Hedgehog yielding a signaling-competent complex. *Science* **362**, eaas8843 (2018).
- Gong, X. et al. Structural basis for the recognition of Sonic Hedgehog by human Patched 1. *Science* **361**, 568 (2018).
- Allen, G. J. & Sanders, D. Two voltage-gated, calcium release channels coreside in the vacuolar membrane of broad bean guard cells. *Plant Cell* **6**, 685–694 (1994).
- Lansman, J. B. Blockade of current through single calcium channels by trivalent lanthanide cations. *Effect of ionic radius on the rates of ion entry and exit.* *J. Gen. Physiol.* **95**, 679–696 (1990).
- Nishitani, W. S., Saif, T. A. & Wang, Y. Calcium signaling in live cells on elastic gels under mechanical vibration at subcellular levels. *PLoS One* **6**, e26181 (2011).
- Liou, J. et al. *STIM* is a  $Ca^{2+}$  sensor essential for  $Ca^{2+}$ -store-depletion-triggered  $Ca^{2+}$  influx. *Curr. Biol.* **15**, 1235–1241 (2005).
- Parekh, A. B. Store-operated CRAC channels: function in health and disease. *Nat. Rev. Drug Discov.* **9**, 399–410 (2010).
- Brandman, O., Liou, J., Park, W. S. & Meyer, T. *STIM2* is a feedback regulator that stabilizes basal cytosolic and endoplasmic reticulum  $Ca^{2+}$  levels. *Cell* **131**, 1327–1339 (2007).
- Lui, R. M., Wang, B., Prakriya, M., Wu, M. M. & Lewis, R. S. Oligomerization of *STIM1* couples ER calcium depletion to CRAC channel activation. *Nature* **454**, 538–542 (2008).
- Luo, C. et al. A genetically encoded ratiometric calcium sensor enables quantitative measurement of the local calcium microdomain in the endoplasmic reticulum. *Biophys. Rep.* **5**, 31–42 (2019).
- Tertyshnikova, S. & Fein, A. Inhibition of inositol 1,4,5-trisphosphate-induced  $Ca^{2+}$  release by cAMP-dependent protein kinase in a living cell. *Proc. Natl. Acad. Sci. USA* **95**, 1613–1617 (1998).
- Belgacem, Y. H. & Borodinsky, L. N. Sonic hedgehog signaling is decoded by calcium spike activity in the developing spinal cord. *Proc. Natl. Acad. Sci. USA* **108**, 4482–4487 (2011).
- Ogden, S. K. et al. G protein Galphai functions immediately downstream of Smoothed in Hedgehog signalling. *Nature* **456**, 967–970 (2008).
- Qi, X. et al. Cryo-EM structure of oxysterol-bound human Smoothed coupled to a heterotrimeric Gi. *Nature* **571**, 279–283 (2019).
- Byrne, E. F. X. et al. Structural basis of Smoothed regulation by its extracellular domains. *Nature* **535**, 517–522 (2016).
- Guadiana, S. M. et al. Arborization of dendrites by developing neocortical neurons is dependent on primary cilia and type 3 adenylyl cyclase. *J. Neurosci.* **33**, 2626–2638 (2013).
- Nachtergaele, S. et al. Oxysterols are allosteric activators of the oncoprotein Smoothed. *Nat. Chem. Biol.* **8**, 211–220 (2012).
- Klatt Shaw, D. et al. Intracellular calcium mobilization is required for Sonic Hedgehog signaling. *Dev. Cell* **45**, 512–525. e5 (2018).
- Moore, B. S. et al. Cilia have high cAMP levels that are inhibited by Sonic Hedgehog-regulated calcium dynamics. *Proc. Natl. Acad. Sci. USA* **113**, 13069–13074 (2016).
- Gwack, Y. et al. Biochemical and functional characterization of *Orai* proteins. *J. Biol. Chem.* **282**, 16232–16243 (2007).
- Zhang, Y. et al. Structural basis for cholesterol transport-like activity of the Hedgehog receptor Patched. *Cell* **175**, 1352–1364. e14 (2018).
- Kinnebrew, M. et al. Patched 1 reduces the accessibility of cholesterol in the outer leaflet of membranes. *eLife* **10**, e70504 (2021).
- Milenkovic, L., Scott, M. P. & Rohatgi, R. Lateral transport of Smoothed from the plasma membrane to the membrane of the cilium. *J. Cell Biol.* **187**, 365–374 (2009).
- Qi, X., Schmiede, P., Coutavas, E., Wang, J. & Li, X. Structures of human Patched and its complex with native palmitoylated sonic hedgehog. *Nature* **560**, 128–132 (2018).
- Hurwitz, S. Homeostatic control of plasma calcium concentration. *Crit. Rev. Biochem. Mol. Biol.* **31**, 41–100 (1996).
- Maxfield, F. R. & Wustner, D. Intracellular cholesterol transport. *J. Clin. Invest.* **110**, 891–898 (2002).
- Albrecht, T., Zhao, Y., Nguyen, T. H., Campbell, R. E. & Johnson, J. D. Fluorescent biosensors illuminate calcium levels within defined beta-cell endosome subpopulations. *Cell Calcium* **57**, 263–274 (2015).
- Myers, B. R., Neahring, L., Zhang, Y., Roberts, K. J. & Beachy, P. A. Rapid, direct activity assays for Smoothed reveal Hedgehog pathway regulation by membrane cholesterol and extracellular sodium. *Proc. Natl. Acad. Sci. USA* **114**, E11141–E11150 (2017).
- Bernatik, O., Paclikova, P., Kotrbova, A., Bryja, V. & Cajanek, L. Primary cilia formation does not rely on WNT/beta-catenin signaling. *Front. Cell Dev. Biol.* **9**, 623753 (2021).
- Zhao, Y., Tong, C. & Jiang, J. Hedgehog regulates smoothed activity by inducing a conformational switch. *Nature* **450**, 252–258 (2007).
- Li, S. et al. Hedgehog-regulated ubiquitination controls smoothed trafficking and cell surface expression in *Drosophila*. *PLoS Biol.* **10**, e1001239 (2012).
- Kim, J. et al. The role of ciliary trafficking in Hedgehog receptor signaling. *Sci. Signal.* **8**, ra55 (2015).
- Kovalchuk, S. I., Jensen, O. N. & Rogowska-Wrzesinska, A. FlashPack: fast and simple preparation of ultrahigh-performance capillary columns for LC-MS. *Mol. Cell Proteomics* **18**, 383–390 (2019).
- Zhou, Y. et al. High-throughput screening of a CRISPR/Cas9 library for functional genomics in human cells. *Nature* **509**, 487–491 (2014).

58. Doench, J. G. et al. Optimized sgRNA design to maximize activity and minimize off-target effects of CRISPR-Cas9. *Nat. Biotechnol.* **34**, 184–191 (2016).
59. Ovchinnikov, D. Alcian blue/alizarin red staining of cartilage and bone in mouse. *Cold Spring Harbor Protocols* **2009**, pdb. prot5170 (2009).
60. Zhao, Y. & Truhlar, D. G. The M06 suite of density functionals for main group thermochemistry, thermochemical kinetics, noncovalent interactions, excited states, and transition elements: two new functionals and systematic testing of four M06-class functionals and 12 other functionals. *Theor. Chem. Accounts* **120**, 215–241 (2008).
61. Frisch M. J. et al. *Gaussian 16, Revision A.03*, (Gaussian, Inc., 2016).

## ACKNOWLEDGEMENTS

We thank Ms. Dan Liang for technical assistance, Dr. Wei Qi (ShanghaiTech University) for revising the manuscript. We appreciate the helpful discussion with Drs. Guo-Yin Yin (Wuhan University) and Yun Zhao (Shanghai Institutes for Biological Sciences). This work was supported by grants from the National Natural Science Foundation of China (22077035, 91753204, 31690102, 91957103), Ministry of Science and Technology of China (2018YFA0800700, 2019YFA0802701), and Fountain-Valley Life Sciences Fund of University of Chinese Academy of Sciences Education Foundation. B.-L.S. acknowledges the support from the Tencent Foundation through the XPLOER PRIZE.

## AUTHOR CONTRIBUTIONS

B.-L.S. conceived the project. J.-Z.Z., C.-C.L, J.W. and W.-W.Q. designed and synthesized cholesterol analogs. A.H. and B.-L.S. designed the experiments. A.H., Z.-C.L., Z.-P.Q., and H.-Y.L. performed the experiments. P.-C.W. performed the structural remodeling. M.Y., G.D. and X.Z. did MS/MS. X.-W.W. and X.H. performed quantum mechanical calculations. A.H. and B.-L.S. analyzed the data. A.H., J.W., W.-W.Q. and B.-L.S. wrote the paper with input from others.

## COMPETING INTERESTS

The authors declare no competing interests.

## ADDITIONAL INFORMATION

**Supplementary information** The online version contains supplementary material available at <https://doi.org/10.1038/s41422-022-00622-0>.

**Correspondence** and requests for materials should be addressed to Xiaolu Zhao, Wen-Wei Qiu or Bao-Liang Song.

**Reprints and permission information** is available at <http://www.nature.com/reprints>